JOURNAL OF CATALYSIS 73, 66–75 (1982)

Adsorption Effects during Temperature-Programmed Desorption of Carbon Monoxide from Supported Platinum

RICHARD K. HERZ, JOANNA B. KIELA, AND SAMUEL P. MARIN

General Motors Research Laboratories, Warren, Michigan 48090

Received April 10, 1981; revised September 3, 1981

Experimental data are presented for the temperature-programmed desorption (TPD) of CO from porous Pt/Al_2O_3 into a vacuum. Most of the preadsorbed CO desorbs in a peak between 380 and 550 K. Other workers have measured desorption at substantially higher temperatures during TPD of CO into a carrier gas rather than a vacuum. A comparison of the experimental conditions suggests that the competition of CO adsorption with CO desorption may contribute to the differences between the TPD results. To investigate the effects of CO adsorption, we develop a mathematical model and use it to compute desorption spectra for the TPD of CO from Pt dispersed over a porous support into (a) an inert carrier gas and (b) a vacuum. Over the realistic parameter range considered, our model predicts that adsorption effects, caused by high concentrations of gaseous CO in the system, are always an important feature, broadening the desorption peaks and shifting them to higher temperatures. Indeed, we find that adsorption competes with desorption to the extent that *adsorption equilibrium* is always approached closely within the porous supported Pt samples. For desorption into a carrier gas, the adsorption effects result from limitations to the flow of CO from the sample cell, whereas for desorption into a vacuum, the adsorption effects result from limitations to the diffusion of CO from the porous sample. Our results suggest that significant adsorption effects will also be present during the TPD of CO from other Group VIII precious metals dispersed over porous supports.

1. INTRODUCTION

Measurements of the temperature-programmed desorption (TPD) of CO from supported metal catalysts can provide information about the strength of interaction of CO with the catalysts. This information contributes to an understanding of such important catalytic processes as CO oxidation, water–gas shift, CO methanation, and the Fischer–Tropsch synthesis. Results have been reported by others for the desorption of CO from Pt (*1–5*), Ni (*6, 7*), and Ru (*8, 9*) dispersed over porous supports. These results are complex and the desorption rates have been analyzed only qualitatively. We are studying the TPD of CO from supported Pt and wish to obtain data that can be analyzed quantitatively.

At the start of our investigation we asked the following question: To what extent will CO adsorption (or "readsorption") during TPD affect our experimental results? The possible presence of adsorption effects has been ignored in previous studies of CO desorption from supported metals with one exception. Low and Bell (*8*) determined that adsorption effects were present during TPD of CO from supported Ru; however, they did not account for these effects when analyzing their data. This somewhat surprising neglect of CO adsorption during TPD from supported metals is probably due to the complexity of this experimental system. Below, we introduce the problems involved in the quantitative analysis of CO desorption from supported Pt and, thus, the problems involved in answering the question posed above. First, however, we provide perspective by considering the TPD (or "thermal desorption") of CO from Pt single crystals.

Results for the TPD of CO from Pt single crystals can be analyzed quantitatively because of the relative simplicity of this experimental system. Since CO is adsorbed

0021-9517/82/010066-10$02.00/0
Copyright © 1982 by Academic Press, Inc.
All rights of reproduction in any form reserved.

on only one crystal plane before an experiment, the resulting TPD "spectrum" will consist of one peak, or a few peaks, corresponding to CO desorption from the limited number of adsorption sites on the crystal plane. In addition, the high gas pumping speed from the UHV sample chamber maintains the CO pressure over the Pt at low values such that the CO adsorption rate during the TPD experiment is negligible with respect to the desorption rate. This feature simplifies considerably the quantitative analysis of the TPD spectrum.

In contrast to the relatively simple CO desorption spectra obtained with Pt crystals (*10*), those obtained for CO desorption from supported Pt (*1–5*) are complex. The TPD spectrum represented by the dashed line in Fig. 1 was obtained by Foger and Anderson (*1*) for the desorption of CO from Pt/Al_2O_3 into flowing He. Foger and Anderson attributed the breadth of the desorption band to the presence in the sample of a distribution of adsorption sites with different CO binding energies. Their explanation is reasonable in view of the complex surface structure of supported metal particles and the possible influence of the oxide support on small metal particles. However, when we (a) used the desorption rate expression obtained by McCabe and Schmidt (*10*) for the most tightly bound state of CO on the crystal planes they studied (their β_H state on the Pt(210) surface), (b) used the 0.58 K s^{-1} heating rate of (*1*), and (c) assumed that the rate of CO adsorption during TPD is negligible (i.e., that no "readsorption" occurs) to compute a TPD spectrum, we obtained a peak at 510 K. Thus, we suspect that some of the desorption that occurred above 510 K in the dashed spectra may have been related to competition between adsorption and desorption caused by the presence of significant CO pressures over the Pt during the experiment.[1] For TPD experiments in general, an increase in the adsorbate pressure at a specified surface coverage and temperature results in an increase in the adsorption rate and, thus, a decrease in the *net* desorption rate (the rate of decrease of surface coverage). This suppression of net desorption rates by increased adsorbate pressures and adsorption rates tends to broaden TPD peaks and shift the peaks to higher temperatures (*12*).

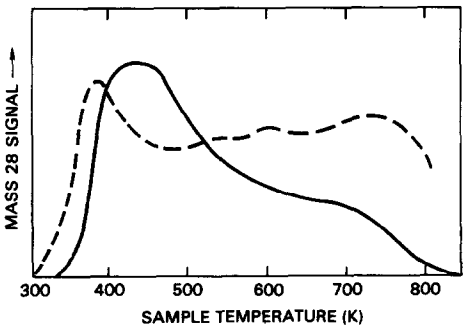

FIG. 1. Dashed curve: data of (*1*) for TPD of CO into flowing He from 0.9 wt% Pt on porous γ-Al_2O_3. Solid curve: TPD of CO into vacuum from 1.0 wt% Pt on porous γ-Al_2O_3. The sample was a 0.015-g, 380-μm thick wafer with a 50-μm chromel–alumel thermocouple embedded at its center. After extensive degassing in vacuum at 850 K, the Pt was saturated with pulses of CO in flowing He at 300 K. Radiant heating in vacuum was linear at 1.1 K s^{-1} from 320 to 850 K. We estimate that temperature gradients within the sample during heating were negligible. Signals at the mass/charge ratios 2, 15, 16, 18, 28, and 44 were measured with a computer-controlled mass spectrometer. The amount of CO_2 that desorbed was about 5% of the amount of CO that desorbed. No significant desorption of H_2, CH_4, or H_2O was detected.

We have attemped to minimize adsorption effects in our experiments by using relatively small amounts of sample and by desorbing CO into a vacuum rather than a carrier gas. The solid curve in Fig. 1 is a typical result. Using the CO capacity of our sample (50 μmol g^{-1}) and the estimated flow rate from the sample cell (800 cm^3 s^{-1}),

[1] As is currently customary in TPD experiments, CO partial pressures were reported on an arbitrary scale in (*1*). We estimate a maximum partial pressure of 1 Torr (1000 ppm) for the dashed spectra in Fig. 1 using the Pt loading (0.9 wt%), Pt dispersion (42%), sample weight (0.5 g), heating rate (0.58 K s^{-1}), and He flow rate, which was not reported in (*1*) but ranged between 0.17 and 0.42 cm^3 s^{-1} in (*11*).

we calculate that the maximum CO pressure over the external surface of the sample was 2×10^{-4} Torr—over three orders of magnitude lower than we estimate was the case for the dashed curve. Although our sample may have had a distribution of CO adsorption sites different from that of the sample used to obtain the dashed spectra, the result that a smaller fraction of CO desorbed above 510 K suggested to us that adsorption effects may have influenced the results of Foger and Anderson. Simple calculations indicated, however, that significant CO pressures may have built up within our sample as a result of the limited rate of diffusion of CO molecules out of the porous support and, thus, that adsorption effects may have influenced our results, to some extent, as well. Further analysis of the extent to which CO adsorption may affect TPD experiments required the use of a mathematical model.

In this paper we formulate a mathematical model of the TPD of CO from supported Pt and use it to simulate two types of systems: desorption into a carrier gas and desorption into a vacuum. We consider desorption from one adsorption state and do not attempt to fit experimental data. The major question we address is: To what extent does adsorption compete with desorption during TPD of CO from Pt dispersed over a porous support? Our simulation results indicate that *adsorption equilibrium* is closely approached over a wide range of conditions. We feel that this result is significant and should be considered in the design, analysis, and reporting of future TPD and temperature-programmed reaction studies of the interaction of CO with supported Pt and other Group VIII precious metals.

In a subsequent paper we will report experiments designed and analyzed with the aid of the mathematical model presented here.

2. THE TPD SYSTEM MODEL

Figure 2 shows a schematic of the desorption system which we intend to model. The slab geometry depicted and the assumed symmetry about the centerline ($x = 0$) reflect our experimental setup.

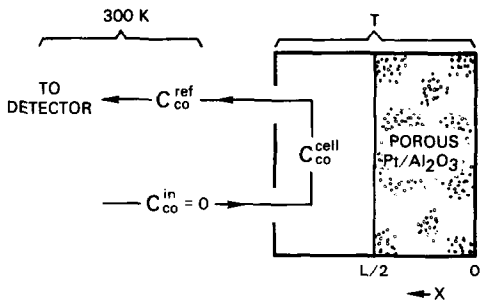

FIG. 2. Schematic representation of a TPD system which contains a porous Pt/Al_2O_3 sample.

We assume that the gas phase in the desorption cell's void volume is well mixed. We neglect CO desorption from the support and specify that CO undergoes only adsorption and desorption over the Pt. If, however, a sample has not been completely dehydrated we find, in agreement with Foger and Anderson (*1*), that significant amounts of CO will desorb as CO_2.

Using these assumptions, we write the following conservation equations for the TPD system:

$$\text{(a)}\quad \frac{dC_{CO}^{cell}}{dt} = -\frac{Q}{V}C_{CO}^{cell} - \frac{AD}{V}\frac{\partial C_{CO}}{\partial x}(L/2, t), \qquad t > 0,$$

$$\text{(b)}\quad \frac{\partial C_{CO}}{\partial t} = \frac{D}{\epsilon}\frac{\partial^2 C_{CO}}{\partial x^2} - \frac{\alpha\mu\rho}{\epsilon}\{r_a - r_d\}, \qquad t > 0,\ 0 < x < L/2,$$

$$\text{(c)}\quad \frac{\partial \theta_{CO}}{\partial t} = r_a - r_d, \qquad t > 0,\ 0 < x < L/2. \quad (2.1)$$

Here, $C_{CO}^{cell}(t)$ is the concentration of CO (mol cm^{-3}) in the cell's void volume at time t, and $C_{CO}(x, t)$ is the concentration of CO in the void space of the porous support at the position x. The variable $\theta_{CO}(x, t)$ is the dimensionless surface concentration of CO and is defined as the ratio of adsorbed CO

molecules to surface Pt atoms (*13*). We assume that the maximum value of θ_{CO} is 1.0 for supported Pt. The remaining problem parameters are defined in the Appendix.

The boundary conditions for Eq. (2.1b) are statements of symmetry at the sample centerline and continuity of gas phase CO concentrations at the sample–void volume interface. These are

$$\frac{\partial C_{CO}}{\partial x}(0, t) = 0, \qquad t > 0,$$

$$C_{CO}(L/2, t) = C_{CO}^{cell}(t), \qquad t > 0. \quad (2.2)$$

Appropriate initial conditions for system (2.1) are

$$C_{CO}^{cell}(0) = 0,$$

$$C_{CO}(x, 0) = 0, \qquad 0 < x < L/2,$$

$$\theta_{CO}(x, 0) = 1, \qquad 0 < x < L/2. \quad (2.3)$$

In each application that follows, the temperature of the sample and desorption cell is specified to increase linearly according to the equation

$$T(t) = T_0 + \beta t, \qquad \text{where } T_0 = 300 \text{ K}, \text{ and } \beta = 1.0 \text{ K s}^{-1}. \quad (2.4)$$

The rates of adsorption (r_a) and desorption (r_d) are given by

$$r_a = F_{CO} S_{CO}(1 - \theta_{CO}), \quad (2.5)$$

$$r_d = k_d \exp(-E_d/RT)\, \theta_{CO}. \quad (2.6)$$

In (2.5), S_{CO} is the initial sticking coefficient of CO on Pt and F_{CO} is the collision frequency of CO molecules with a Pt atom:

$$F_{CO} = (RT/2\pi M_{CO})^{1/2} \sigma C_{CO}. \quad (2.7)$$

Here, R is the ideal gas constant, M_{CO} is the molecular weight of CO, and σ is the area occupied by one mole of surface Pt atoms (4.03×10^8 cm^2 mol^{-1}).

There is clearly some uncertainty associated with the specification of expressions (2.5)–(2.7) and with the selection of the parameters S_{CO}, k_d, and E_d. Since our purpose here is to investigate the effects of CO adsorption on TPD results rather than to predict actual results, we have used simple rate expressions and rounded values of the rate parameters (Table 1) to compute the results presented below. Our previous kinetic study (*13*) and experimental TPD results indicate that our choices are sufficiently realistic for the present purpose. As we discuss at the end of Section 3, the conclusions of this work hold over a wide range of S_{CO}, k_d, E_d, and β. While we specifically consider Pt here, we note that all of the Group VIII precious metals have similar CO sticking coefficients and adsorption energies (*14*).

For our calculations, the values used for cell volume, carrier gas flow rate, vacuum pumping speed, sample dimensions, Pt loading, and sample weight are within the ranges reported in published TPD studies. Mercury porosimetry measurements on our TPD samples were used to obtain ρ (density), ϵ (void fraction), and the macropore and micropore radii and volumes. These radius and volume measurements were used to estimate the effective diffusion

TABLE 1

Parameter Values Used to Compute TPD Spectra

A (cm^2)	varied[a]
D_{300} (cm^2 s^{-1}) carrier gas:	0.040
vacuum:	0.066
L (cm)	varied[b]
Q_{300} (cm^3 s^{-1})	varied[b]
V (cm^3)	5.0
α	0.8
ϵ	0.58
μ (mol g^{-1})	4×10^{-5} [c]
ρ (g cm^{-3})	1.25
T_0 (K)	300
β (K s^{-1})	1.0
E_d (kcal mol^{-1})	30[d]
k_d (s^{-1})	10^{13}
S_{CO}	0.5

[a] Selected to keep the sample weight at 0.2 g for desorption into a carrier gas and 0.01 g for desorption into a vacuum.

[b] Values given in captions of Figs. 3 and 4.

[c] Equivalent to 1 wt% Pt.

[d] 126 kJ mol^{-1}.

coefficient D by means of a random pore model (*15*). In our estimation of D for desorption into a carrier gas we assumed that binary diffusion of CO in He at 1 atm occurs in the sample's macropores, whereas for desorption into a vacuum we assumed that Knudsen diffusion of CO occurs in the macropores. Numerical solutions of the system (2.1)–(2.3) were obtained using software developed by Madsen and Sincovec (*16*).

3. MODEL APPLICATIONS

A. *Desorption into an Inert Carrier Gas*

For TPD into a carrier gas we assume that the volumetric flow rate, Q, from the cell, increases with temperature according to

$$Q = Q_{300}\left(\frac{T}{300\ \text{K}}\right), \qquad (3.1)$$

where Q_{300} is the flow rate at the initial temperature of 300 K. For our TPD samples the temperature dependence of the effective diffusion coefficient is given by

$$D = D_{300}\left(\frac{T}{300\ \text{K}}\right)^{0.7}. \qquad (3.2)$$

Using the parameter values shown in Table 1, Eqs. (2.1)–(2.3) were solved to give $C_{\text{CO}}^{\text{cell}}(t)$, $C_{\text{CO}}(x, t)$, and $\theta_{\text{CO}}(x, t)$. Our plots, however, display the reference concentration $C_{\text{CO}}^{\text{ref}}(t)$, the concentration of CO in the carrier gas at the inlet to the detector (often a mass spectrometer). We specify that the temperature of the gas at the detector inlet is 300 K and neglect the time required for flow from the cell outlet to the detector inlet. $C_{\text{CO}}^{\text{ref}}(t)$ is obtained from $C_{\text{CO}}^{\text{cell}}(t)$ according to

$$C_{\text{CO}}^{\text{ref}}(t) = C_{\text{CO}}^{\text{cell}}(t)\left(\frac{T(t)}{300\ \text{K}}\right). \qquad (3.3)$$

Plots of $C_{\text{CO}}^{\text{ref}}(t)$ vs $T(t)$ are shown in Fig. 3 for the six cases defined in the figure caption. In addition to a scale with units of (mol cm^{-3}), the graph also contains the scale of the mole fraction of CO in the carrier gas, X_{CO}, with units (ppm).

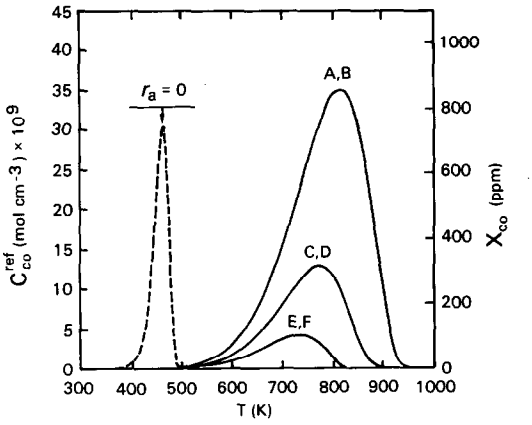

FIG. 3. Numerical simulation of the TPD of CO from porous Pt/Al_2O_3 into an inert carrier gas. The dashed peak is on an arbitrary scale and represents the hypothetical result that would be obtained if the rate of adsorption of CO (r_a) were zero. The solid curves were computed using the parameter values listed in Table 1 and below. (A) $L = 20\ \mu\text{m}$, $Q = 1\ \text{cm}^3\ \text{s}^{-1}$; (B) $L = 200\ \mu\text{m}$, $Q = 1\ \text{cm}^3\ \text{s}^{-1}$; (C) $L = 20\ \mu\text{m}$, $Q = 3\ \text{cm}^3\ \text{s}^{-1}$; (D) $L = 200\ \mu\text{m}$, $Q = 3\ \text{cm}^3\ \text{s}^{-1}$; (E) $L = 20\ \mu\text{m}$, $Q = 10\ \text{cm}^3\ \text{s}^{-1}$; (F) $L = 200\ \mu\text{m}$, $Q = 10\ \text{cm}^3\ \text{s}^{-1}$.

Our first remarks about the cases shown in Fig. 3 concern the degree to which adsorption competed with desorption during these simulated TPD experiments. We found, when we varied both S_{CO} and k_d while keeping their ratio constant, that the desorption spectra did not change significantly. This observation remained valid when S_{CO} and k_d were both multiplied or divided by as much as 5. Thus, over the parameter range considered (cases A through F in Fig. 3), adsorption competed with desorption to the extent that adsorption equilibrium was closely approached for all $t > 0$. This means that the results of experiments performed under similar conditions can be used to determine only the CO adsorption equilibrium "constant" and heat of adsorption (e.g., by the method described by Cvetanovic and Amenomiya (*12*)) but not the separate adsorption and desorption rate parameters. For CO on Pt, however, the heat of adsorption may closely approximate E_d since the adsorption of CO on Pt apparently is not activated

(*17, 18*). This relationship between the heat of adsorption and E_d may also hold for many other adsorption systems.

The extent to which adsorption, in competition with desorption, affected the shapes and locations of the peaks can be seen by comparing the solid curves in Fig. 3 with the dashed curve (which is shown on a different, arbitrary scale). The dashed curve is proportional to the limiting result that would be obtained if the concentration of gaseous CO is maintained at very low levels such that the adsorption rate remains negligibly small with respect to the desorption rate. This curve was computed simply by setting r_a to zero. Since we determined that there are no significant time lags in this system due to the rate of accumulation of gaseous CO within the cell and sample, the temperature corresponding to the maximum of the dashed peak is the same as that calculated from β, k_d, and E_d using Redhead's method (*19*).

Our next remarks concern the effects of sample thickness and flow rate variation. The influence of internal mass transfer by diffusion was assessed by varying sample thickness while maintaining constant sample weight. Two sample thicknesses were chosen and desorption spectra were obtained at different flow rates. The almost identical results obtained with the two thicknesses demonstrate that internal mass transfer effects were not significant for the cases considered here. Centerline concentrations, $C_{CO}(0, t)$, differed by only a few percent from the concentrations at the sample face, $C_{CO}(L/2, t)$. The largest difference at a peak maximum occurred in case F where the difference was about 5%.

As the flow rate was increased (e.g., in the sequence A, C, E in Fig. 3), the concentration of gaseous CO over the Pt in the sample decreased and the peaks shifted to lower temperatures. Similar effects were observed when the amount of Pt in the system was decreased while the flow rate was held constant. Thus, the results of these simulated experiments were controlled by the relatively high levels of gaseous CO in the cell established as a result of the relatively low flow rates and large sample amounts used.

We note, as did Cvetanovic and Amenomiya (*12*), that peak positions exhibit only minor sensitivity to flow rate variations. If, as is commonly done, flow rate variations are used to test for the presence of significant adsorption effects, then one must ensure that a sufficiently wide range of flow rates is used.

Attempts to eliminate significant adsorption effects in this setting by increasing the flow rate and decreasing the amount of Pt in the system will be limited by the sensitivity of the detector. For example, we have estimated for mass spectrometric analysis that the practical limit of detectability of CO (when $M_{CO} = 28$) in an inert gas at 1 atm is about 25 ppm. Because of this limitation it is unlikely that adsorption effects can be made negligible for TPD into a carrier gas.

B. Desorption into a Vacuum

In this case we specify that the volumetric flow rate from the cell, Q, and the diffusion coefficient, D, are temperature-dependent according to the following equations

$$Q = Q_{300}\left(\frac{T}{300\ \text{K}}\right)^{1/2}, \tag{3.4}$$

$$D = D_{300}\left(\frac{T}{300\ \text{K}}\right)^{1/2}. \tag{3.5}$$

This temperature dependence is explained by the fact that, in vacuum, free molecular flow occurs in the cell and in both the macropores and micropores of the sample (i.e., Knudsen diffusion occurs exclusively within the sample).

This case applies to an experimental system which differs somewhat from the system represented by Fig. 2. For desorption into a vacuum, there is no inlet flow and the sample cell is connected to and pumped by a vacuum chamber that contains the detector, a mass spectrometer, and is at ambient temperature (300 K).

We will plot a reference concentration, C_{CO}^{ref}, which is proportional to the mass spectrometer signal, C_{CO}^{det}, but which is independent of the flow rate from the mass spectrometer chamber, Q_{300}^{det}. This reference concentration is obtained by multiplying C_{CO}^{det} by the ratio of the flow rate from the mass spectrometer chamber to the flow rate from the cell at 300 K. We have

$$C_{CO}^{ref} = C_{CO}^{det}(Q_{300}^{det}/Q_{300}^{cell}). \quad (3.6)$$

To relate C_{CO}^{ref} to the computed quantity C_{CO}^{cell}, we note that, since

$$C_{CO}^{det} = C_{CO}^{cell}(Q_T^{cell}/Q_{300}^{det}) = C_{CO}^{cell}(Q_{300}^{cell}/Q_{300}^{det})(T/300\ \text{K})^{1/2}, \quad (3.7)$$

Eq. (3.6) is equivalent to

$$C_{CO}^{ref} = C_{CO}^{cell}\left(\frac{T}{300\ \text{K}}\right)^{1/2}. \quad (3.8)$$

Again, we neglect the time required for flow from the cell through the mass spectrometer chamber.

Simulation results displayed in Fig. 4 use the parameter values listed in Table 1 and in the figure caption. The plots of $C_{CO}^{ref}(t)$ vs $T(t)$ in Fig. 4 are shown relative to two scales: one giving C_{CO}^{ref} in units (mol cm^{-3}) and the other giving equivalent partial pressures (P_{CO}^{ref}) in units (Torr).

Before examining the simulation results we remark that eliminating the carrier gas by desorbing into a vacuum allows lower CO concentrations to be measured with a mass spectrometer. Eliminating the carrier gas, however, introduces new experimental problems. The carrier gas serves as a heat transfer agent and its absence makes temperature measurement and uniform heating of the porous insulating support material difficult. Fortunately these problems can be solved by careful experimental design, for example, by embedding a thermocouple in the adsorbent sample and heating the sample radiantly (*20*).

An examination of the plots in Fig. 4 reveals first that, although the flow rates are much higher and the sample weight much lower than for TPD into a carrier gas, there

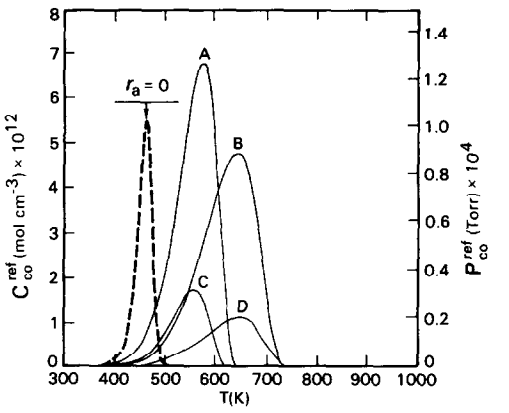

FIG. 4. Numerical simulation of the TPD of CO from porous Pt/Al_2O_3 into a vacuum. The dashed peak is on an arbitrary scale and represents the hypothetical result that would be obtained if the rate of adsorption of CO (r_a) were zero. The solid curves were computed using the parameter values listed in Table 1 and below. (A) $L = 20\ \mu$m, $Q = 500$ cm^3 s^{-1}; (B) $L = 200\ \mu$m, $Q = 500$ cm^3 s^{-1}; (C) $L = 20\ \mu$m, $Q = 2000$ cm^3 s^{-1}; (D) $L = 200\ \mu$m, $Q = 2000$ cm^3 s^{-1}.

are still large adsorption effects. These effects result primarily from the accumulation of gaseous CO within the sample caused by the limited rate of diffusion of CO out of the sample. These diffusion effects are illustrated by the shift of the peaks to lower temperatures as the sample thickness was decreased. They are also illustrated by comparing the concentrations at the centerline ($x = 0$) to those at the sample face ($x = L/2$). We list these values in Table 2 at the temperatures T_M corresponding to the peak maxima.

Variation of S_{CO} and k_d again demonstrated that local adsorption equilibrium was closely approached for the cases shown in Fig. 4. This was true even though there were large concentration gradients present within the sample, and the behavior persisted when S_{CO} and k_d were multiplied or divided by as much as 10. Cvetanovic and Amenomiya (*12*) have analyzed a similar TPD system in which internal diffusion control, adsorption equilibrium, and a linear adsorption isotherm were specified. They found that the heat of adsorption can be determined by varying the heating rate, as

TABLE 2

Concentrations and Temperatures at the Peak Maxima for the Cases of Fig. 4

Case	$C_{CO}(0, T_M)$ (mol cm^{-3})	$C_{CO}(L/2, T_M)$ (mol cm^{-3})	T_M (K)
A	7.2×10^{-12}	4.9×10^{-12}	573
B	1.7×10^{-10}	3.3×10^{-12}	639
C	3.8×10^{-12}	1.3×10^{-12}	555
D	1.5×10^{-10}	0.8×10^{-12}	636

in the case of desorption with negligible diffusional effects. Although the adsorption isotherm considered here is nonlinear, the slope of a plot of $\ln(T_M^2/\beta)$ vs $(1/T_M)$ is (E_d/R), where T_M were obtained from spectra computed for β between 0.2 and 1.0 K s^{-1}.

Close, local approach to adsorption equilibrium during TPD also was obtained for case C in Fig. 4 (and, thus, would be obtained for all other cases in Figs. 3 and 4) for a wide range of parameter values: S_{CO} = 0.1 to 1.0, $k_d = 10^{13}$ to 10^{19} s^{-1}, E_d = 19 to 30 kcal mol^{-1}, and β = 0.1 to 1.0 s^{-1}. In addition, this result was obtained when we used the initial sticking coefficients and coverage-dependent desorption rate expressions reported by McCabe and Schmidt (*10*) for the (111) and (110) planes of Pt crystals. CO is held less strongly on these crystal planes than on the other planes studied in (*10*).

As in Fig. 3, the dashed curve in Fig. 4 (which again is on an arbitrary scale) is the result that would be obtained if the concentration of gaseous CO is maintained at very low levels such that the adsorption rate remains negligibly small with respect to the desorption rate. In theory, this limiting result could be approached with an infinitesimal sample thickness and a very large flow rate. In practice, we feel that adsorption effects cannot be eliminated for the TPD of CO from Pt dispersed over a porous support. The limiting result of TPD with negligible adsorption effects might be approachable for the desorption of CO from a metal dispersed over a nonporous support, a system studied by Poppa *et al.* (*21–23*).

4. SUMMARY

Our results indicate that adsorption effects may be difficult or impossible to eliminate during TPD of CO from Pt dispersed over porous supports. At low flow rates (desorption into a carrier gas), the accumulation of gaseous CO in the sample cell controls the results, whereas at high flow rates (desorption into a vacuum), the accumulation of gaseous CO within the sample that results from diffusional limitations becomes controlling. For all of the cases considered here, adsorption competed with desorption to the extent that adsorption equilibrium was closely approached at each point in a sample. Thus, the results of TPD experiments performed under these conditions can be used to determine the ratios of the adsorption and desorption rate parameters for a specified adsorption model but not the separate desorption rate parameters.

The results presented here do not explain all of the features of our experimental TPD spectra or of those reported by others. These results do, however, emphasize the need to consider adsorption effects when designing experiments, analyzing data, and reporting results. We recommend that all of the extensive parameters of a TPD system be reported (including flow rates and dimensions of adsorbent particles) and that concentration or partial pressure scales be shown on plots of TPD spectra. While we have specifically considered the TPD of CO from supported Pt, our results suggest that significant adsorption effects will also be present during the TPD of CO from other Group VIII precious metals dispersed over porous supports.

APPENDIX: NOMENCLATURE

A Total external (geometric) surface area of the sample (cm^2).

C_{CO} Concentration of CO in the gas phase within the porous sample (mol cm^{-3}).

C_{CO}^{cell} Concentration of CO in the gas phase of the desorption cell external to the sample (mol cm^{-3}).

C_{CO}^{det} Concentration of CO in the detector chamber for desorption into vacuum (mol cm^{-3}).

C_{CO}^{ref} Concentration of CO at the reference conditions specified in the text (mol cm^{-3}).

D Effective diffusion coefficient of CO within the porous sample at the temperature T (cm^2 s^{-1}).

D_{300} Effective diffusion coefficient of CO within the porous sample at 300 K (cm^2 s^{-1}).

E_d Activation energy for desorption of CO (kJ mol^{-1}).

F_{CO} Frequency of collision of gas phase CO molecules with surface Pt atoms (s^{-1}).

k_d Preexponential rate constant for desorption of CO (s^{-1}).

L Total thickness of the sample (cm).

M_{CO} Molecular weight of CO (g mol^{-1}).

P_{CO}^{ref} Partial pressure of CO at the reference conditions specified in the text for desorption into vacuum (Torr).

Q, Q_T^{cell} Volumetric flow rate of gas from the cell at the temperature T (cm^3 s^{-1}).

Q_{300}, Q_{300}^{cell} Volumetric flow rate of gas from the cell at 300 K (cm^3 s^{-1}).

Q_{300}^{det} Volumetric flow rate of gas from the detector chamber at 300 K for desorption into vacuum (cm^3 s^{-1}).

r_a Rate of adsorption of CO (s^{-1}).

r_d Rate of desorption of CO (s^{-1}).

R Ideal gas constant (8.3144×10^7 g cm^2 s^{-2} mol^{-1} K^{-1}) or (1.9873×10^{-3} kcal mol^{-1} K^{-1}).

S_{CO} Initial sticking coefficient of CO on Pt (dimensionless).

t Time (s)

T Temperature of the sample and desorption cell (K).

T_0 Temperature of the sample and desorption cell at $t = 0$ (K).

T_M Temperature at which the maximum of a desorption peak occurs (K).

V Volume of the void space external to the sample in the desorption cell (cm^3).

x Distance from the center of the sample (cm).

X_{CO} Mole fraction of CO in the carrier gas (ppm).

Greek symbols

α Fraction of the Pt atoms in the sample that are exposed to the gas phase (dimensionless).

β Rate of temperature increase (K s^{-1}).

ϵ Void fraction of the porous sample (dimensionless).

θ_{CO} Surface concentration of CO: the ratio of adsorbed CO molecules to surface Pt atoms (dimensionless).

μ Molar loading of Pt per gram of sample (mol g^{-1}).

ρ Apparent density of the sample (g cm^{-3}).

σ Area occupied by one mole of surface Pt atoms (4.03×10^8 cm^2 mol^{-1}).

ACKNOWLEDGMENT

Mr. David F. McCready performed the TPD experiments.

REFERENCES

1. Foger, K., and Anderson, J. R., *Appl. Surf. Sci.* **2**, 335 (1979).
2. Komers, R., Amenomiya, Y., and Cvetanovic, R. J., *J. Catal.* **15**, 293 (1969).
3. Cvetanovic, R. J., and Amenomiya, Y., *Catal. Rev.* **6**, 21 (1972).
4. Bain, F. T., Jackson, S. D., Thomson, S. J., Webb, G., and Willocks, E., *J. Chem. Soc. Faraday 1* **72**, 2516 (1976).

5. Hoang-Van, C., Ghorbel, A., Pommier, B., and Teichner, S. J., *Bull. Soc. Chim. Fr.* **1976,** 355 (1976).
6. Zagli, A. E., Falconer, J. L., and Keenan, C. A., *J. Catal.* **56,** 453 (1979).
7. Falconer, J. L., and Zagli, A. E., *J. Catal.* **62,** 280 (1980).
8. Low, G. G., and Bell, A. T., *J. Catal.* **57,** 397 (1979).
9. Fujimoto, K., Kameyama, M., and Kunugi, T., *J. Catal.* **61,** 7 (1980).
10. McCabe, R. W., and Schmidt, L. D., *Surf. Sci.* **66,** 101 (1977).
11. Anderson, J. R., Foger, K., and Breakspere, R. J., *J. Catal.* **57,** 458 (1979).
12. Cvetanovic, R. J., and Amenomiya, Y., *Advan. Catal.* **17,** 103 (1967).
13. Herz, R. K., and Marin, S. P., *J. Catal.* **65,** 281 (1980).
14. Engel, T., and Ertl, G., *Advan. Catal.* **28,** 1 (1979).
15. Smith, J. M., "Chemical Engineering Kinetics," 2nd ed., p. 414. McGraw–Hill, New York, 1970.
16. Madsen, N. K., and Sincovec, R. F., *Assoc. Comput. Mach. Trans. Math. Software* **5,** 326 (1979).
17. Campbell, C. T., Ertl, G., Kuipers, H., and Segner, J., *Surf. Sci.* **107,** 207 (1981).
18. Shigeishi, R. A., and King, D. A., *Surf. Sci.* **58,** 379 (1976).
19. Redhead, P. A., *Vacuum* **12,** 203 (1962).
20. Halpern, B., and Germain, J. E., *J. Catal.* **37,** 44 (1975).
21. Thomas, M. E., Poppa, H., and Pound, G. M., *Thin Solid Films* **58,** 273 (1979).
22. Doering, D. L., Poppa, H., and Dickinson, J. T., *J. Vac. Sci. Technol.* **17,** 198 (1980).
23. Lada, S., Poppa, H., and Boudart, M., *Surf. Sci.* **102,** 151 (1981).